Metal–Organic Pathways for Anisotropic Growth of a Highly Symmetrical Crystal Structure: Example of the fcc Ni

ARTICLE *in* LANGMUIR · AUGUST 2013

Impact Factor: 4.46 · DOI: 10.1021/la402001t · Source: PubMed

5 AUTHORS, INCLUDING:

Stefanos Mourdikoudis
Pierre and Marie Curie University - Paris 6
26 PUBLICATIONS **349** CITATIONS
SEE PROFILE

Catherine Amiens
Paul Sabatier University - Toulouse III
99 PUBLICATIONS **3,562** CITATIONS
SEE PROFILE

Langmuir

Article

pubs.acs.org/Langmuir

Metal−Organic Pathways for Anisotropic Growth of a Highly Symmetrical Crystal Structure: Example of the fcc Ni

Stefanos Mourdikoudis, Vincent Collière, Catherine Amiens, Pierre Fau,* and Myrtil L. Kahn*

Laboratoire de Chimie de Coordination, CNRS UPR8241, 205, route de Narbonne, 31077 Toulouse, France

Supporting Information

ABSTRACT: The control of the metallic nanocrystal shape is of prime importance for a wide variety of applications. We report a detailed research work on metal−organic chemical routes for the synthesis of a highly symmetrical crystal structure. In particular, this study shows the key parameters ensuring the anisotropic growth of nickel nanostructures (fcc crystal). Numerous reaction conditions are investigated (precursors, solvents, temperature, reducing agents, reaction time, and types and ratios of surfactants, such as alkyl amines, carboxylic acids, and phosphine oxides), and their effects on the size and shape of the final product are reported. The role of the growth modifiers and the structuring of the reaction media on the anisotropic growth are demonstrated. This metal−organic approach generates several novel anisotropic nanostructures in a wide size range depending on the reaction conditions. In this way, nanomaterials with reproducible size, shape, and composition are obtained with good yield. Transmission electron microscopy techniques (TEM and HRTEM) are the principal methods for monitoring the morphology.

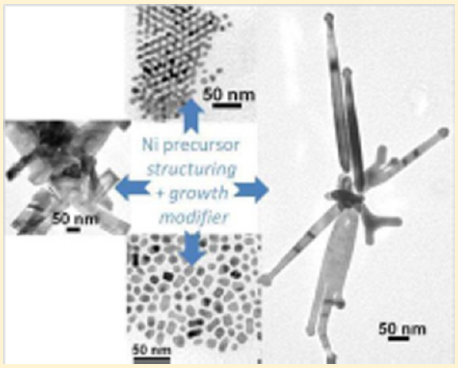

INTRODUCTION

Tailoring the morphology of a metallic nanocrystal is critical to modern materials chemistry. Indeed, designing the morphology can render them candidate materials for a wide variety of applications (e.g., catalysis, electronics, magnetic devices, semiconduction and optics, sensing, biodiagnostics, etc.)[1−8] Nickel nanocrystals are in that respect a remarkable example of a truly multifunctional material based only on their shape control. For example, the magnetization saturation of cubic shaped nickel nanoparticles (NPs) is 10-fold higher that of spherical nanoparticles with similar size.[9] Nickel nanostrands (micrometer long nickel wires) are currently employed for producing electrically conductive carbon composites in advanced airplane structures.[10] The morphology of the nanomaterials, however, depends closely on the synthetic method. The optimized performance and the full exploitation of nanomaterials is, as a consequence, directly related to a successful and reproducible synthetic procedure.

Because of the intrinsic face-centered-cubic (fcc) crystal structure of Ni, the formation of highly anisotropic morphologies is not as straightforward as for metals with an inherently anisotropic crystal structure, e.g., hexagonal (hCP) cobalt or zinc. So far, only few examples have been reported for the preparation of anisotropic Ni nanostructures. From the standpoint of a wet synthetic procedure, the preparation of Ni NPs can de divided into two main streams: one relies on the decomposition of nickel salts (chloride, nitrates, etc.) in water based medium, in the presence or not of surfactants.[11] The second stream corresponds to the synthesis of Ni NPs in organic medium. In the first case, where the syntheses are performed in water, micrometer long nanowires can be achieved through the mechanism of oriented attachment of the pristine Ni NPs triggered by chloride anions.[12] Ni nanowires were also prepared using hydrazine in water in the presence of an external magnetic field. In this case, Zhang and co-workers noted that in the absence of a magnetic field no nanowires were formed.[13] Depending on the reaction conditions, various shapes have been described. Ni nanobelts were produced by reducing $NiCl_2{\cdot}6H_2O$ with $NaH_2PO_2{\cdot}H_2O$ in aqueous medium in the presence of $Na_2C_4H_4O_6$, NaOH, and sodium dodecyl benzenesulfonate.[14] The reduction of $NiCl_2{\cdot}6H_2O$ by hydrazine monohydrate in ethylene glycol, in the presence of PVP, led to the production of Ni nanochains.[15] Nanostars and "flower-shaped" microparticles were prepared by the treatment of $Ni(acetate)_2$ with hydrazine monohydrate in water in the presence of NaOH.[16,17]

On the other hand, the synthesis of Ni NPs in organic medium is much less described although it may offer "cleaner" reaction conditions, i.e., halide-free systems. Metal−organic chemistry is, in that respect, an efficient approach for the preparation of metallic or metal oxide nanostructures of controlled size and shape.[18−22] The combination of reaction conditions (e.g., the nature and concentration of the stabilizing agents, the organometallic precursors, the solvents, and the reducing agents) plays a crucial role in growth control.[23] The choice of temperature and reaction time is also important for

Received: May 27, 2013
Revised: July 25, 2013
Published: July 26, 2013

obtaining homogeneous nanostructures. When focusing on Ni structures prepared in organic medium, the most frequently reported end-products are isotropic particles. These shapes (spheres or cubes) correspond to thermodynamically stable geometries. A literature survey highlights that such structures are generally obtained when amine and/*or* phosphine are used as surfactants. Carenco et al. have published a systematic study on the effect of the simultaneous presence of oleylamine (OAm) and trioctylphosphine (TOP) during the decomposition of $Ni(acac)_2$, managing to produce monodisperse isotropic particles in the 2−30 mn size range.[24] The relative amounts of the above ligands were found to affect drastically the final mean size, size distribution, shape, and aggregation state of the particles. Anisotropic Ni structures have also been described; for example, Ni nanorods have been obtained through the hydrogenolysis of organometallic Ni precursors.[25−27] Hexagonal and triangular Ni nanoplates have been prepared via the reduction of Ni-formate in 1-octadecene.[28] Urchin-like morphologies, nanochains, hollow-shapes, nanotriangles, nanospikes, and monodisperse nanocubes have been reported.[9,29−32] In such cases, the chemical synthesis of metallic nanocrystals is usually presented to occur in three distinct stages: (1) nucleation, (2) evolution of nuclei into seeds, and (3) growth of the seeds into nanocrystals.[33] The growth process leading to anisotropic particles remains still somewhat unclear in such conditions. It is generally reported to take place by the coalescence of initially formed seeds in a privileged direction resulting either from a preferred coordination of ligands on specific faces or from the formation of a "soft" template matrix in solution due to the presence of the stabilizing agents. In any case, this necessitates the ability of metallic particles to coalesce in the conditions of organic solution chemistry.[34]

In the present work, we report an extensive study on the chemical synthesis of nickel nanostructures in organic medium displaying numerous different morphologies, such as monodisperse spherical nanoparticles, nanorods, nanoknives, nanoplanes, nanotripods, nanowires, and nanokites. We investigated a great number of nickel precursors, solvents, surfactants, reducing agents, and temperatures, achieving the production of a large variety of Ni nanostructures. The results of this extended synthetic work allow us to gain a better understanding of several key parameters responsible for the shape control of Ni nanoparticles in organic medium. In particular, we have found that the right choice of the combination of the nickel precursor/additional ligand is a key factor for a good structuring of the reaction media. Finally, appropriate growth modifiers for the anisotropic growth control of such a highly symmetrical crystal structure are proposed.

RESULTS

The general synthetic route explored in this study is illustrated in Scheme 1:

Scheme 1. Synthetic Route

$$[NiL_aX_b] \xrightarrow[\text{Solvent, x SA}]{H_2} Ni.\,x\ SA$$

$[NiL_aX_b]$ = $Ni(COD)_2$, $Ni(acac)_2$, $Ni(OOCCH_3)_2$, $Ni(OOC(CH_2)_{16}CH_3)_2$
SA = RNH_2 and/or R'COOH, TOPO, TPPO
Solvent = Anisole, Hexadecane

Synthesis and Morphology. All synthetic protocols presented here are one-pot reactions. Since the superparamagnetic limit for Ni is ca. 8 nm[35,36] and most of the samples reported in this work have a nanoparticle size above this value, ferromagnetic products were obtained and collected on the stirring magnet at the end of the reaction, simplifying the washing procedure. Typically black powders were isolated after removal of the supernatant, pentane precipitation, and a final wash with THF. Drying under dynamic vacuum was followed by the recovery of the powder in a glovebox, with the help of a strong permanent magnet. By variation of the experimental parameters such as the nickel precursors, solvents, surfactants, reducing agents, and temperatures, isotropic (Table 1) or anisotropic (Table 2) Ni structures were obtained. In the following, the samples are categorized depending on their shape highlightening the experimental parameters of importance for the achievement of a good shape control. Discussion of the results presented in the current section will be provided in the respective Discussion section.

Isotropic Ni Nanoparticles. When $Ni(COD)_2$ is decomposed at 150 °C under H_2 in anisole in the presence of oleic acid and oleylamine, nanoparticles with a bimodal size distribution are obtained. For example, small isotropic particles with an average size of 8(1) nm and large particles of 26(4) nm are obtained for a reaction time of 48 h (sample IS1, Figure S1a in the Supporting Information). Applying 1-week heating time provides a similar morphology pattern: 8(1) nm and 30(7) nm particles (sample IS2, Figure S1b).

When $Ni(COD)_2$ is decomposed at 150 °C under H_2 for 48 h in pure oleylamine, monodisperse spherical particles (7(1) nm) that self-assemble in fine arrays upon the evaporation of the solvent on the TEM grid are obtained (Figure 1a, sample IS3). If the decomposition of $Ni(COD)_2$ is performed using the same experimental conditions but at 215 °C for 1 h, isotropic particles with a size around 4 nm are observed, together with the sporadic presence of ∼10 nm particles (Supporting Information, Figure S2, sample IS9). Isotropic nanoparticles (4(1) nm) are also obtained when $Ni(COD)_2$ is decomposed at 150 °C under H_2 for 48 h in anisole in the presence of 12 equivalents (equiv.) of oleylamine (sample IS8, Figure S3) or when $Ni(COD)_2$ is decomposed at 120 °C under H_2 for 48 h in ethylenediamine (10(2) nm; Figure S4, sample IS4). The use of $Ni(acac)_2$ in the same experimental conditions also leads to isotropic nanoparticles (6(1) nm; sample IS6, Figure S5). Using Ni-stearate [i.e., $Ni(OOC(CH_2)_{16}CH_3)_2$] yields isotropic particles (9(2) nm) in pure oleylamine only when the reaction mixture is postheated at 250 °C for 1 h (sample IS5, Figure S6). Smaller nanoparticles (3(1) nm) are obtained when $Ni(COD)_2$ is decomposed at 150 °C under H_2 for 48 h in pure trioctylamine (TOAm), a bulky molecule, but a few areas of the grid were covered by larger aggregates (sample IS7, Figure S7).

When $Ni(COD)_2$ is decomposed at 150 °C under H_2 in anisole in the presence of both 1-adamantanecarboxylic acid (ACA) and hexadecylamine (HDA), isotropic nanoparticles of 8(1) nm are observed (Figure 1b, sample IS10). Such morphology is acquired for specific relative concentrations of the ligands (i.e., 1 equiv. ACA/2 equiv. HDA to 1 equiv. of metal), but such ratio did not always lead to well-defined homogeneous particles. For instance, when Ni-acetate [i.e., $Ni(OOCCH_3)_2$] is reduced at 215 °C under H_2 in hexadecane for 1h in the presence of both ACA and HDA (1/2 ACA/HDA ratio), isotropic nanoparticles of around 3 nm are produced

dx.doi.org/10.1021/la402001t | *Langmuir* 2013, 29, 13491−13501

Table 1. Summary of the Experimental Conditions for the Isotropic Nickel Samples [*] IS5[a]

sample code	precursor	ligand(s) (ratio)	solvent	T (°C)	t (h)	average size (nm), population	Figure
IS1	$Ni(COD)_2$	OAc/OAm (2/1)	anisole	150	48	26(4), 35% and 8(1), 65%	S1a
IS2	$Ni(COD)_2$	OAc/OAm (2/1)	anisole	150	168	30(7), 20% and 8(1), 80%	S1b
IS3	$Ni(COD)_2$		OAm	150	48	7(1)	1a
IS4	$Ni(COD)_2$		EDA	120	48	10(2)	S4
IS5[*]	Ni-stearate		OAm	150/250	48/1	9(2)	S6
IS6	$Ni(acac)_2$		EDA	120	48	6(1)	S5
IS7	$Ni(COD)_2$		TOAm	150	48	3(0.5)	S7
IS8	$Ni(COD)_2$	OAm (12 equiv)	anisole	150	48	4(1)	S3
IS9	$Ni(COD)_2$		OAm	215	1	4(1), 8% and 10(2), 92%	S2
IS10	$Ni(COD)_2$	ACA/HDA (1/2)	anisole	150	24	8(1)	1b
IS11	Ni-acetate	ACA/HDA (1/2)	hexadecane	215	1	3(0.6), 70% and aggregates, 30%	S8

[a]Synthesis performed at 150 °C for 48 h followed by 1 h at 250 °C.

together with some agglomerates formed from ca. 11 nm-sized particles (Figure S8, sample IS11).

Anisotropic Ni Nanostructures. When Ni-stearate is reduced at 150 °C under H_2 in anisole for 48 h in the presence of HDA, nickel nanorods with an aspect ratio of ca. 10 (length $l \approx 250$ nm, thickness $d \approx 25$ nm) are obtained. Similar results are acquired if this reaction is performed under vigorous magnetic stirring (sample AN1 in Figure 2a) or without magnetic stirring (sample AN10, Figure S9). In the latter case, a less homogeneous product is obtained although the tendency for anisotropic shape is still observed. Modification of the concentration (half solvent quantity) leads also to nanorods (sample AN9, Figure S10). However, when ACA is used as a coligand, submicrometer plane-like structures are obtained (sample AN21, Figure 2b).

When $Ni(acac)_2$ or $Ni(OOCCH_3)_2$ is reduced at 150 °C under H_2 in anisole for 48 h in the presence of ACA and HDA (1/2 ratio), nanoknives are obtained ($d \approx 40$ nm in their main body length, Figure S11, sample AN23 and Figure S12, sample AN22 respectively), while an inversed (2/1) ACA/HDA ratio changes radically the morphology, providing smooth-angled ~50 nm structures (Figure S13, sample AN24). The use of $Ni(COD)_2$ leads to ~40 nm nanoparticles with a polygonal shape (Figure S14, sample AN25). Note that the single use of ACA as ligand induces the formation of large aggregates (Figure S15, sample AG1).

When Ni-stearate is reduced at 150 °C under H_2 for 48 h in pure OAm, large multipods together with small particles (~7 nm) are formed (Figure S16, sample AN2). When $Ni(OOCCH_3)_2$ or $Ni(acac)_2$ are used instead of the Ni-stearate precursor, multiangular nanostructures with sizes in the range of ca. 60−100 nm (Figure S17, sample AN7) or multipod like-anisotropic structures with an average size of ~15 nm (Figure S18, sample AN3) are obtained, respectively. When $Ni(acac)_2$ is reduced at 150 °C under H_2 for 48 h in anisole in the presence of oleic acid/oleylamine (2/1 ratio), large polygonal morphologies such as triagonal and hexagonal submicrometer structures with an average size of ca. 250−300 nm are obtained (Figure S19, sample AN5). When $Ni(acac)_2$ is reduced at 150 °C under H_2 for 48 h in anisole in the presence of HDA, nanorods with an average length of ~65 nm and a diameter of ~20 nm (Figure S20, sample AN4) are acquired. However, the use of $Ni(OOCCH_3)_2$, keeping the rest reaction parameters unchanged, leads to the formation of "nanovessels" with length of about ~150 nm and thickness of ~40−50 nm (sample AN6, Figure S21).

When Ni-stearate is decomposed at 150 °C under H_2 in ODA for 48 h, nanorod-like structures with a length around ~300 nm and a diameter of ~25 nm are obtained (sample AN8, Figure 3a). Keeping similar reaction conditions, but replacing ODA by HDA, provides elongated morphologies (sample AN28, Figure S22). When $Ni(COD)_2$ is decomposed at 150 °C under H_2 in TOPO for 48 h, nanodiabolos (~40 nm size, sample AN30, Figure S23) together with some small particles with size lower than 10 nm are obtained.

When $Ni(OOCCH_3)_2$ is reduced at 215 °C under H_2 in OAm for 1 h, anisotropic shapes with a size ca. ~100 nm (sample AN11, Figure S24) are obtained. The presence of 2 equiv. of HDA leads to less agglomerated particles (sample AN12, Figure 3b), while oleic acid does not cause any important change at the morphology of the product (Figure S25, sample AN15). The use of ACA induces the formation of large and sharp anisotropic structures (Figure 3c, sample AN20). The employment of pure HDA does not improve the agglomeration state (sample AN16, Figure S26), while the use of $Ni(acac)_2$ in HDA leads to ~50 nm polygonal particles with a fair degree of separation (sample AN17, Figure S27). As well, when $Ni(acac)_2$ is reduced at 215 °C under H_2 in OAm for 1 h, multipod structures are produced (Figure S28, sample AN13). However, less homogeneous nanostructures are obtained using the Ni-stearate precursor in the above conditions (Figure S29, sample AN14).

When $Ni(OOCCH_3)_2$ is reduced at 215 °C under H_2 in OAm for 1h, in the presence of triphenylphosphine oxide (TPPO, 10 equiv.), nanokites of ~120−140 nm in size are obtained (sample AN18, Figure 3d). Employing TOPO instead of TPPO modified only slightly the shape of the product (sample AN26, Figure S30). On the other hand, the use of TPPO at lower temperature (150 °C, 48 h), results in more aggregated structures (sample AN29, Figure S31).

When $Ni(OOCCH_3)_2$ is reduced at 215 °C under H_2 in hexadecane for 1h in the presence of 2 equiv. of HDA, long nanowires (micrometer scale length − thickness between 70 and 130 nm (Figure S32, AN19)) and few particles are obtained. Increasing the HDA concentration leads to polygonal-like particles (50−60 nm in size, Figure S33, sample AN27).

Characterization. The reaction conditions described herein facilitate the acquisition of oxide-free nickel nanostructures. All samples were stored in an Ar-filled glovebox after the preparation. In most cases, the strong attraction of the product on the stirring magnet, a pure room-temperature ferromagnetic behavior, is indicative of the metallic character of the sample.

dx.doi.org/10.1021/la402001t | Langmuir 2013, 29, 13491−13501

Table 2. Summary of the Reaction Parameters for All Anisotropic Nickel Samples Produced[a]

sample	precursor	ligands	solvent	T (°C)	t (h)	morphology, shape yield	size (nm)	Figure
AN1	Ni-stearate	HDA (2 equiv)	anisole	150	48	nanorods, 100%	$l \approx 250(25)$ and $d \approx 25(3)$	2a
AN2	Ni-stearate		OAm	150	48	multipods, 50% and NPs, 50%	multipods, $l \approx 100(40)$ and NPs, d ≈ 7(1)	S16
AN3	$Ni(acac)_2$		OAm	150	48	nanotripods, 80%	15(3)	S18
AN4	$Ni(acac)_2$	HDA	anisole	150	48	nanorods, 70%	$l \approx 65(18)$, $d \approx 20(5)$	S20
AN5	$Ni(acac)_2$	OAc/OAm 2/1	anisole	150	48	nanohexagons, 60%, nanotriangles, 30%	hexagons 255(35) and triangles 275(30)	S19
AN6	Ni-acetate	HDA	anisole	150	48	nanovessels, 90%	$l \approx 150(20)$, $d \approx 45(10)$	S21
AN7	Ni-acetate		OAm	150	48	multiangular, 100%	80(25)	S17
AN8	Ni-stearate		ODA	150	48	nanorods, 95%	$l \approx 300(35)$, $d \approx 25(3)$	3a
AN9	Ni-stearate	HDA	anisole	150	48	nanorods, 100%	$l \approx 250(25)$, $d \approx 25(3)$	S10
AN10	Ni-stearate	HDA	anisole	150	48	nanorods, 80%	$l \approx 220(55)$, $d \approx 18(5)$	S9
AN11	Ni-acetate		OAm	215	1	multiangular, 80%	100(25)	S24
AN12	Ni-acetate	HDA (2 equiv)	OAm	215	1	"3d" multiangular, 90%	125(36)	3b
AN13	$Ni(acac)_2$		OAm	215	1	multipods, 75%	225(40)	S28
AN14	Ni-stearate		OAm	215	1	aggregated anisotropic NPs, 100%	aggregates consisted of NPs of size 150(50)	S29
AN15	Ni-acetate	OAc (2 equiv)	OAm	215	1	multiangular, 100%	130(45)	S25
AN16	Ni-acetate		HDA	215	1	aggregates of polyponal NPs, 100%	aggregates of NPs of $d \approx 67(22)$	S26
AN17	$Ni(acac)_2$		HDA	215	1	nanopolygons, 80%	~50(16)	S27
AN18	Ni-acetate	TPPO (10 equiv)	OAm	215	1	nanokites, 70%	130(20)	3d
AN19	Ni-acetate	HDA (2 equiv)	hexadecane	215	1	nanowires, 60% and NPs, 40%	NWs $l > 1$ μm, $d \approx 100(35)$ and NPs, $d \approx 170(45)$	S32
AN20	Ni-acetate	ACA (2 equiv)	OAm	215	1	"sharp" anisotropic structures, 95%	$l \approx 950(180)$, $d \approx 100(16)$	3c
AN21	Ni-stearate	ACA/HDA (1/2)	anisole	150	48	"plane-like" nanostructures, 80%	$h \approx 250(33)$, $w \approx 600(72)$, $d \approx 90(21)$	2b
AN22	Ni-acetate	ACA/HDA (1/2)	anisole	150	24	nanoknives, 80%	$l \approx 200(35)$, $d \approx 40(13)$	S12
AN23	$Ni(acac)_2$	ACA/HDA (1/2)	anisole	150	24	nanoknives, 75%	$l \approx 200(28)$, $d \approx 40(11)$	S11
AN24	Ni-acetate	ACA/HDA (2/1)	anisole	150	24	smooth-angled nanopolygons, 80%	~50(14)	S13
AN25	$Ni(COD)_2$	ACA/HDA (2/1)	anisole	150	24	smooth-angled nanopolygons, 85%	~40(13)	S14
AN26	Ni-acetate	TOPO (10 equiv)	OAm	215	1	multiangular structures, 80%	~200(45)	S30
AN27	Ni-acetate	HDA (10 equiv)	hexadecane	215	1	polygon-like shape, 95%	55(8)	S33
AN28	Ni-stearate		HDA	150	48	elongated shape, 70%	$l \approx 280(32)$, $d \approx 27(3)$	S22
AN29	Ni-acetate	TPPO (10 equiv)	OAm	150	48	aggregated multiangular structures, 100%	aggregates consisted of multiangular structures of size ~200(40)	S31
AN30	$Ni(COD)_2$		TOPO	150	48	nanodiabolos, 70% and NPs, 30%	nanodiabolos of size ~40(6) and NPs of size ~9(2)	S23
AG1	$Ni(COD)_2$	ACA (1 equiv)	anisole	150	24	large aggregates, 100%	size grows uncontrollably	S15

[a]Sample codes AN1−AN30: anisotropic shapes; AG1: completely aggregated configuration. Refer to the Experimental Section for further details.

The efficiency of our synthesis approach is confirmed by elemental analysis exhibiting a metal content of ca. 90% for all samples studied.

As a typical example, the XRD pattern of sample AN1 is displayed in Figure 4a. This diffractogram is characteristic of a highly crystalline sample. Peaks at 44.5, 51.8, and 76.4° can be attributed to the (111), (200), and (220) lattice planes of fcc-Ni (JCPDS-04−0850), respectively. fcc-Ni peaks are also evidenced for the sample AN30 which contains a mix of anisotropic and isotropic particles. No hcp-Ni peaks can be detected (Figure S35 in the Supporting Information).

High-resolution transmission electron microscopy measurements strengthened the clues for fcc-Ni structure. Inverse-Fourier-transformed images evidence a d-spacing of 0.203 nm in agreement with the (111) lattice plane of the cubic Ni phase, for two distinct samples (Figure 4c for sample AN1 and Figure S34 for sample AN22). The monocrystalline character of our nanomaterials is moreover evidenced. In particular, the orientation of the "nanoknife" in its upper part (Figure S34, sample AN22 in the Supporting Information) remains intact compared to the main body of this structure.

The FTIR spectra verify the existence of ligands at the surface of the Ni even after the washing procedure. For example, two bands at 3317 and 1635 cm^{-1}, attributed to the surface-capping hexadecylamine surfactant and its N−H stretching and bending modes, respectively, are observed for

dx.doi.org/10.1021/la402001t | Langmuir 2013, 29, 13491−13501

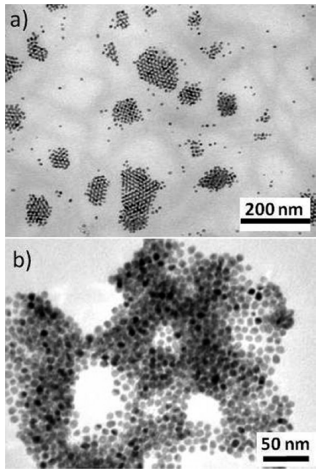

Figure 1. TEM image of (a) sample IS3 and (b) sample IS10.

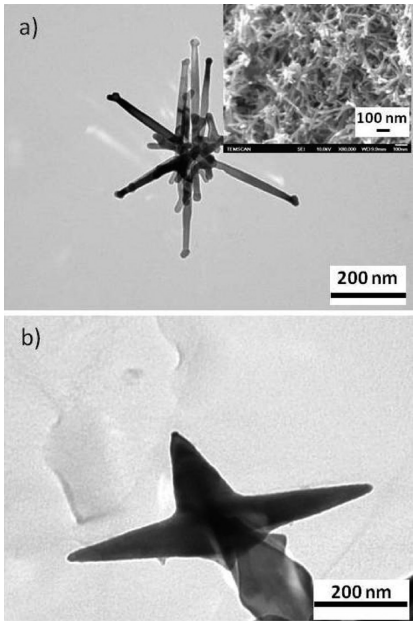

Figure 2. (a) Decomposition of Ni-stearate for 48 h in anisole under magnetic stirring, sample AN1 (SEM image at the inset), and (b) TEM image of sample AN21.

sample AN1 (Figure 4b). The two bands at 1547 and 1414 cm^{-1} indicate unidentate attachment of the stearate anion to the surface. Unidentate binding is further supported from the difference $\Delta\nu = \nu_{asym} - \nu_{sym}$ (1547−1414 = 133 cm^{-1}) between the asymmetrical and symmetrical stretching modes of the stearate ligand. The bands at 2920 and 2852 cm^{-1} (stretching mode) and at 1467 cm^{-1} (scissoring mode) are assigned to the methylene moieties in the aliphatic chain of the capping ligands.[37]

The ferromagnetic properties are evidenced by the strong tendency of the as-prepared powders to readily stick on the stirring magnet after the end of reaction and the termination of stirring conditions. M-H plots (Figure 4d) acquired by SQuID measurements provide a saturation magnetization of ca. 51 emu/g_{Ni} (A m^{-1} g_{Ni}^{-1}). This value is close to the saturation magnetization of the bulk Ni (ca. 55 emu/g). The anisotropic shape of the samples induces usually a higher coercivity than the one of the bulk Ni (0.7 Oe). For example, a coercivity of ca.

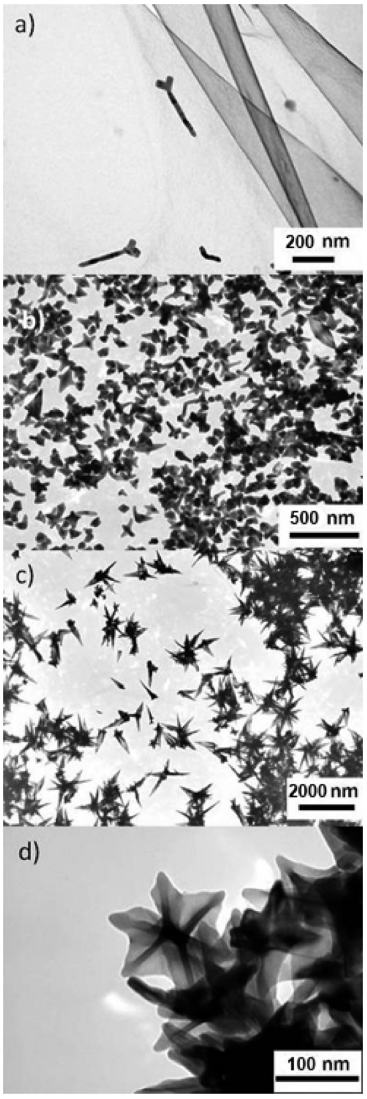

Figure 3. (a) TEM image of sample AN8, (b) sample AN12, (c) sample AN20, and (d) sample AN18.

155 Oe is measured at 300 K for sample AN1. We have previously demonstrated that while carbon monoxide, trioctylphosphine oxide, or methanol could greatly decrease the magnetic moment of the surface atoms, amines and carboxylic acids did not alter it.[26]

DISCUSSION

Isotropic Ni NPs. Even if the synthesis of isotropic NPs may appear simple, their preparation is not always straightforward (multimodal populations can be obtained, samples IS1, IS2, and IS9). Our study shows that different chemical pathways can lead to isotropic growth, but the "quality" of the NPs (i.e., controlled mean size and low size distribution) can be obtained only by reproducing protocols under strict synthetic conditions. In each case, it is important to select not only suitable ligands or precursors but also the combinations between all synthetic parameters and the way in which the chemicals are added. One feature of high quality NPs is their propensity to self-assemble in two-dimensional or three-dimensional arrays. Sample IS3 is characteristic of such high quality NPs. Very homogeneous particles with a mean size of 7 nm and a size dispersion as low as 1 nm (standard deviation)

dx.doi.org/10.1021/la402001t | *Langmuir* 2013, 29, 13491−13501

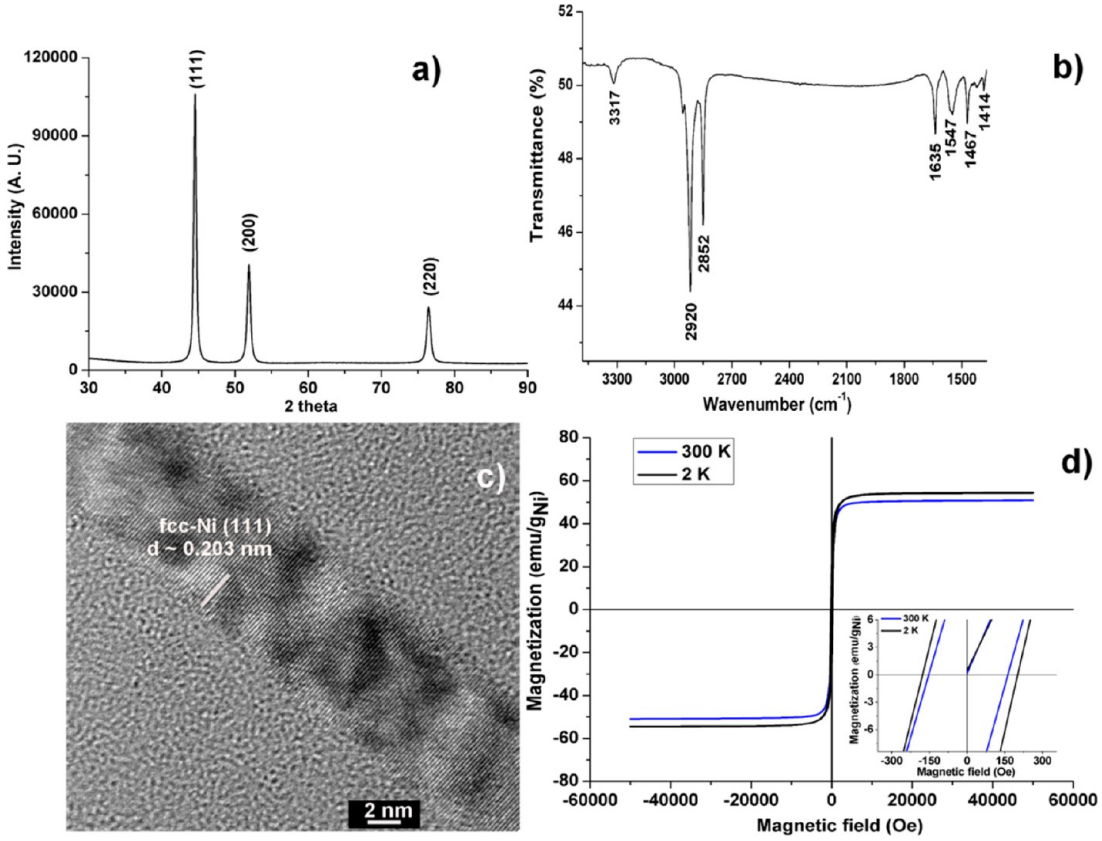

Figure 4. (a) XRD measurement of the sample AN1, (b) FTIR spectrum for sample AN1, (c) HRTEM image for the nanorods of the sample AN1, and (d) hysteresis loops for sample AN1, measured by SQuID magnetometer at 2 and 300 K. The inset in the bottom-right part is an enlargement for lower magnetic field values.

displaying 2D and 3D organizations are obtained. However, we observed that the optimum assembly of the Ni NPs on the microscopy grid is obtained not only when the NPs are monodisperse but also when they are stabilized with long alkyl chains (C18 for OAm) which allow a strong hydrophobic interaction between the particles (see IS6 and IS3 for comparison). The best conditions for the preparation of homogeneously distributed Ni particles are: a Ni precursor with low decomposition temperature like $Ni(COD)_2$, the use of a moderate reaction temperature, and the presence of an excess of amine ligands with a long alkyl chain (C18).

IS3, IS4, and IS7 illustrate how different amine ligands [respectively OAm, EDA(ethylenediamine), and TOAm] can modify the final size and size distribution of the NPs. We observed that a bulky tertiary amine (TOAm) leads to smaller NPs (sample IS7, mean size 3 nm) than the ones obtained with primary amines (either long alkyl chain or bidentate amines). This result is in agreement with a previous work reported by Donegan and co-workers showing that bulky alkylamine ligands lead to smaller Ni NPs.[38]

Anisotropic Ni Nanostructures. The achievement of anisotropic growth for Ni nanostructures is really challenging as Ni naturally adopts the highly symmetrical fcc crystal structure, which does not possess any inherent anisotropy. As an illustration, keeping the otherwise same synthesis conditions as for sample IS1, but replacing $Ni(COD)_2$ by Co(COD)-(COT), a metal with an anisotropic hcp crystal structure, results in the growth of Co nanowires ($d \approx 8$ nm, $l \approx 1$ μm).[39]

The shapes of crystals are controlled by a combination of energetic and kinetic factors.[40,41] The modification of the crystal shapes (even crystals with highly symmetrical crystal structure) is enabled by introducing growth modifiers (like ions or molecules).[40−42] Gold is, in that respect, a very convincing example. It has been frequently demonstrated that the presence of Ag^+ ions (growth modifiers) in the reaction medium is necessary to achieve Au nanorods.[43] As well, an aurophilic bonding-assisted growth mechanism relying on cooperative interaction, organization and reaction between inorganic precursor salts and oleylamine has been reported for the growth of Au nanowires.[44] However, a literature survey shows that one ligand may be an efficient growth modifier for a given metal but can seem to be inefficient for another one. For example, our study shows that EDA does not favor anisotropic growth of Ni in contrast to what has been observed for FePt,[45] CoPt,[46] Cu,[47] and Pt[48] for which diamine ligands have been considered as responsible for the synthesis of anisotropic materials by their specific coordination to Cu or Pt.

In this study, we have investigated the introduction of the coordinating ligand (i.e., growth modifier) either by its direct introduction in the reaction solution or by an indirect addition via the decomposition of the Ni precursor. Upon decomposition, the precursor releases coordinating ligands over time. As a general trend, isotropic NPs were obtained when $Ni(COD)_2$ was used (refer to Table 1 and Table 2). The two exceptions, AN25 and AN30, are, in fact, samples with only smooth anisotropic shapes. Clearly, $Ni(COD)_2$ easily leads to metallic crystals, the shape of which corresponds to the thermodynamic equilibrium. Surprisingly, as long as the Ni precursor is different and the applied coordinating ligand is released during precursor decomposition, anisotropic structures

dx.doi.org/10.1021/la402001t | Langmuir 2013, 29, 13491−13501

are obtained (see as examples IS3, AN3 and AN7, or IS1 and AN5). Of course, nickel acetylacetonate, nickel acetate, and Ni-stearate decompose differently than $Ni(COD)_2$;[49] but our study demonstrates that the releasable ligand itself is of major importance. For instance, different morphologies are obtained when $Ni(stearate)_2$ or $Ni(acetate)_2$ (two Ni(II) precursors with "comparable" ligand shell, i.e., with a comparable decomposition mechanism) are used (see for example AN1 and AN6).

Among all tested synthetic conditions, the one involving $Ni(stearate)_2$ in the presence of HDA in anisole (AN1) appears to be the most efficient and robust method to achieve homogeneous anisotropic growth of Ni. Indeed, nanorods with an aspect ratio of ~10 (mean length 250 nm, mean diameter 25 nm) are obtained. Using double the Ni(II) concentration did not cause a particular modification of the rods morphology similarly to the application (or not) of stirring during the reaction (see experimental part, samples AN1, AN9, and AN10). The necessary use of dihydrogen as a reducing agent for the synthesis of metallic Ni at a relatively low temperature (150 °C) was proved when we tried to carry out the same reaction using carbon monoxide, an alternative gaseous reducing agent: no nanostructures were obtained. Besides, the use of simply inert conditions in the reaction pot (Ar atmosphere instead of H_2) could not allow $Ni(stearate)_2$ decomposition.

Varying the Ni precursor without modifying the rest of the reaction parameters used for sample AN1 yields also anisotropic structures but with a lower control of morphology. In particular the structures are less homogeneous when $Ni(acac)_2$ and $Ni(acetate)_2$ are used (AN4 and AN6, respectively). The stearate moiety must obviously play a crucial role for the homogeneous anisotropic growth control through participation in a structuring effect of the reaction media via van der Walls interactions between the alkyl chains of the ligands. Such structuring effect (i.e., soft template) may however be difficult to characterize by classical methods (like SAXS and/or SANS) as it may be dynamic (e.g., correlated to the kinetics of the precursor decomposition) and not necessarily occur in a long-range.

On the other hand, if the above hypothesis is correct, experiments performed at high temperature should lead to the loss of the structuring of the reaction medium and eventually to the formation of rather isotropic structures. Experimentally, at much higher temperatures, we no longer get anisotropic particles but only spherical ones (sample IS5). This result is in agreement with literature data for Rh and Pt nanostructures prepared in OAm[50,51] or for hcp Ni structures prepared at 290 °C with ACA/OAm ligands.[52] In these cases, spherical or nearly spherical particles were formed under high temperature conditions, while lower temperatures favored the formation of more anisotropic structures. Besides, if the procedure includes heating at 215 °C (a temperature chosen to avoid the synthesis of hcp-Ni, which can take place at higher temperatures)[53] for 1 h (a short reaction time) under hydrogen atmosphere,[54] anisotropic structures are recovered (AN11 and AN13). However, even if these structures are similar to AN7, we notice a considerable size increase maintaining a common preference for multiangular shape growth. These results show clearly that the temperature is too high for the media to be well structured and only smooth anisotropic forms are obtained. It is thus necessary to ensure the employement of both a suitable growth modifier and a good structuring of the reaction medium to achieve an homogeneous anisotropic growth of Ni. The above result has to be related with the classic thermal decomposition approach for which it is usually admitted that the higher temperature often provides an environment to obtain nanocrystals with better crystallinity. Nevertheless, strong heating conditions can also increase the solubility of monomers, weaken the surfactants binding strength, and also eventually lead to the loss of the structuring of the media. Our study therefore highlights that the achievement of a controlled anisotropic growth necessitates the use of moderate temperatures to avoid the loss of the structuring effect. In the same context, a small modification at the ligand, like the amine, can influence the final morphology of Ni nanomaterials. For example, the exclusive use of long-alkyl-chain amines as octadecylamine and hexadecylamine (two quite similar ligands) leads to rods (AN8 and AN28) comparable to AN1. On the other hand, heterogeneous anisotropic structures are observed applying an otherwise similar protocol but replacing the aforementioned amines with sole OAm (AN2). The double C═C bond in the middle of the OAm molecular chain together with the 'buckled' chain configuration may induce a different organization of the reaction medium compared to ODA and HDA.

Several other ligands were also tested as growth modifiers. Ligands such as TOAm, TPPO, and TOPO appear as less interesting growth modifiers (samples IS7, AN18, AN26, AN29, and AN30). In these cases, Ni structures with extended aggregation or inhomogeneous shapes have been obtained. These results are in contrast to the ones reported for CdS where the combination of TOPO and OAm led to the formation of anisotropic nanocrystals (nanorods, bipods, tripods).[55] These ligands taken alone, although so efficient for the anisotropic growth of hcp crystal structures, are apparently not that sufficient in the case of fcc ones. A tendency for anisotropic growth is nevertheless still observed in our case, even in the absence of polymorphism (i.e., simultaneous presence of fcc- and hcp-Ni phases) contrary to what has been very recently proposed for anisotropic (branch- and rod-like) growth.[56] Moreover, if we compare the samples AN30 and IS3, for which only the solvent is modified (TOPO instead of OAm, respectively) quite different morphologies are obtained. Such a result is related to the inherent differences between TOPO and OAm. As reasonable hypothesis, the observed modifications at the particles morphologies can be attributed to features such as: the voluminous molecule of TOPO, compared to the linear OAm and/or the π-acceptor capability of TOPO in contrast to OAm which is a σ-donor species.[27]

ACA ligand (a voluminous molecule without particular molecular organization properties) appears to be a good candidate as a growth modifier as previously suggested for Fe_3O_4 and $CoPt_3$ structures.[57,58] It has to be noted that with the $Ni(COD)_2$ precursor the use of ACA as the sole coordinating molecule leads to large aggregates (AG1). In that case, a rapid nucleation and aggregation process occurs, with a poor stabilization effect of the carboxylic function of the ligand. The addition of ACA in the stearate-HDA ligand mixture seems to provoke a very different growth mechanism since large nanoplane morphologies (AN21) were formed. The importance of the acid/amine relative concentration with respect to the final particle morphology is well illustrated by the comparison of AN22 and AN24. This general tendency is observed regardless of the Ni precursor (samples AN21-AN25).

dx.doi.org/10.1021/la402001t | Langmuir 2013, 29, 13491−13501

In particular, the 1/2 ACA/HDA ratio provided spherical nanoparticles using $Ni(COD)_2$ as the nickel source (IS10), while keeping the same precursor but inversing the ACA/HDA ratio to 2/1 led to larger smoothly anisotropic particles (AN25). This result constitutes a clear example of how an excess of the bulky ACA molecule can protect a population of surface sites from being coordinated with surfactant molecules, thus yielding particles with relatively larger sizes and with shapes different than the thermodynamically favored isotropic ones.[57] Regarding the use of acetate- and acetylacetonate precursors, while the 2/1 proportion of ACA/HDA leads to smooth-angled nanopolygons (e.g., AN24), the 1/2 proportion results in "nanoknife" structures (samples AN22 and AN23). Peculiar-shaped structures with a "sharp" morphology and larger size are observed when inserting ACA in OAm (sample AN20), which is a somewhat different behavior compared to the exclusive use of OAm during the decomposition of Ni-acetate (sample AN11).

To summarize, these results demonstrate that the formation of anisotropic Ni structures is easily achieved through the hydrogenolysis of Ni precursors and the careful control of the reaction conditions. Deciphering the exact role of each parameter on the growth control of the crystals in solution is not trivial work. Nevertheless, we have shed some light on the synthesis process of various anisotropic nanostructures, referring to the Ni nanorods as one of our best examples. The latter anisotropic structures have been generated by the hydrogen reduction of the Ni-stearate precursor, employed in combination with long chain alkylamines and at a moderate temperature (150 °C). These conditions provide a favorable environment for the structuring of the medium around the crystal during its growth leading to the formation of monodisperse Ni nanorods with a high aspect ratio. Finally, we have to note that the different synthetic conditions explored herein lead to diverse decomposition behaviors that undoubtedly affect at the outset of nucleation and growth stages. Shen et al. have shown that the properties of such nuclei (size, shape, surface effects, and presence of any possible structural defects) are also important regarding the control of the final anisotropic shape, especially via an oriented-attachment mechanism.[59] At this stage, no evidence of such an oriented-attachment mechanism has yet been shown in this study. A future focus on the role of such in situ formed nanoseeds would be worth to study for several nanoparticle systems.

CONCLUSIONS

The morphology control of a highly symmetrical crystal structure like fcc-Ni at the nanoscale has been achieved through a metal−organic approach. The tuning of the reaction parameters allows to produce a variety of morphologies such as nanorods, nanokites and nanoknives or self-assembled isotropic Ni particles. Significant information concerning the role of each one of the factors that influence the final shape has been proposed. Even though the growth mechanisms are not yet completely clear and remain under investigation, this study illustrates that the structuring of the reaction media as well as the introduction of appropriate growth modifiers are key drivers for the anisotropic growth control of such a highly symmetrical crystal structure. These results may be of particular importance for certain applications in fields as catalysis, conducting transparent electrodes, or composite materials with enhanced electrical conductivity.

EXPERIMENTAL SECTION

All operations were carried out using standard Schlenk techniques (Ar-filled glovebox, vacuum-line, Schlenk tubes) and Fischer−Porter bottles, which allow the application of an inert or reducing atmosphere during synthesis but also throughout the pre- and postpreparation handling of the materials.

Materials. Anhydrous anisole solvent (99.7%, Sigma-Aldrich) was distilled over sodium and degassed by a three-cycle freeze−thaw process before use. Pentane and THF were collected after going through drying columns (MB-SPS-800 solvent purification system). All reactants (oleylamine, 80−90% C18, 97% primary amines, Acros Organics; octadecylamine ≥99.0%, Aldrich; hexadecylamine 98%, Aldrich; trioctylamine 98%, Fluka; ethylenediamine 99%, Fluka; triphenylphosphine oxide 98%, Fluka; trioctylphosphine oxide 99%, Aldrich; oleic acid 99%, Aldrich; 1-adamantanecarboxylic acid 99%, Aldrich; $Ni(COD)_2$ 98%, Strem; Ni(II) acetylacetonate 98%, Strem; Ni(II) acetate tetrahydrate 98%, Strem; nickel stearate, Strem) were entered inside a glovebox (O_2 < 1 ppm, H_2O < 1 ppm) as received, without any further purification, to be weighed while avoiding any oxygen or water contamination. Dihydrogen (Air Liquide) contained less than 5 ppm O_2 and 5 ppm H_2O.

Specimens for TEM were prepared by slow evaporation of a drop of each colloidal suspension deposited onto a carbon-covered Cu grid. The TEM observations were performed at the "Service Commun de Microscopie Electronique de l'Université Paul Sabatier" (TEMSCAN) in Toulouse on a JEOL JEM 1011 transmission electron microscope operating at 100 kV with resolution of 4.5 Å. The HRTEM images were acquired on a JEOL JEM 2100F TEM-FEG operating at 200 kV with resolution of 2.3 Å and they were analyzed by Gatan Digital Micrograph software. The SEM analyses were carried out in a JEOL JSM 6700F. Infrared spectra were recorded on a Perkin-Elmer Spectrum 100 FT-IR spectrometer using KBr pellets after isolation of the products as solids. X-ray powder-diffraction patterns were measured by a Panalytical MPDPro diffractometer, using Cu Kα radiation (1.54059 Å). Samples for XRD measurements were sealed in 0.5 mm-diameter Lindemann glass capillaries. The magnetic properties were investigated by the use of a SQuID magnetometer MPMS5, able to carry out measurements at the 2−400 K temperature range and under a magnetic field up to 5T. Elemental analyses were performed by the "Service de microanalyses du Laboratoire de Chimie de Coordination" (C, H, and N) or by Antellis Co. (Ni).

Preparation of nickel nanostructures (refer to Tables 1 and 2 for all samples, with further classification to isotropic, anisotropic and aggregated samples): Sample IS1: 564 mg (2 mmol) of oleic acid and 0.33 mL (1 mmol) of oleylamine were dissolved in 20 mL of anisole. After 10 min stirring, this solution was transferred via a canula into a Fischer−Porter bottle containing 275 mg (1 mmol) of $Ni(COD)_2$. The mixture was stirred for 20 min to give a dark yellow-orange solution. Argon was then evacuated, and the bottle was pressurized under 3 bar of H_2 for 20 min, placed into a preheated oil bath at 150 °C and stirred for 48 h. During this time the color of the solution changed to dark brown-black. At the end of the reaction, the dihydrogen was evacuated, and the solution was left to cool to room temperature. The final product was recovered after filtration and dried under dynamic vacuum overnight.

IS2: As in sample IS1, but with one week of reaction instead of 48 h.

AN1: In a Fischer−Porter bottle containing 60 mL of anisole, 6 mmol (1.446 g) of hexadecylamine (HDA) and 3 mmol (1.875 g) of Nickel(II)-stearate were inserted to afford a light green color. After 20 min of hydrogenation (3 bar) the bottle was placed in an oil bath at 150 °C for 48 h, under intermediate magnetic stirring (~700 rpm). In the end of the reaction, almost all of the precursor was decomposed, the color of the solution became transparent, and the solid ferromagnetic product was collected on the stirring magnet. The H_2 was evacuated, and the bottle was filled with Ar. A canula was used to remove the hot anisole-hexadecylamine mixture. The product was left to cool and dry as usual (room temperature, dynamic vacuum). If the final nanomaterial seems to have a high organic content (not

sufficiently black-colored powder), a canula-wash with pentane and then with THF is recommended before drying.

IS3: 1 mmol of $Ni(COD)_2$ diluted in excess oleylamine (30 mL) and decomposed under 3 bar H_2 at 150 °C for 48 h.

AN2: As in IS3 but now using Ni-stearate instead of $Ni(COD)_2$.

IS4: As in IS3, but now ethylenediamine is used instead of oleylamine. Heating at 120 °C.

IS5: As in AN2, but now the bottle was further heated to 250 °C for 1 h.

AN3: As in IS3, but $Ni(acac)_2$ replaced the $Ni(COD)_2$ precursor.

IS6: As in IS4, but $Ni(acac)_2$ replaced the $Ni(COD)_2$ precursor.

AN4: As in AN1, but $Ni(acac)_2$ replaced the Ni-stearate.

AN5: As in IS1, but $Ni(acac)_2$ replaced the $Ni(COD)_2$.

AN6: As in AN1 or AN4, but now Ni-acetate was used as a precursor.

AN7: As in IS3 or AN3, but now Ni-acetate was used as a precursor.

AN8: As in AN2, but now Ni-stearate was decomposed in excess octadecylamine, instead of oleylamine.

AN9: As in AN1, but now half quantity of anisole was used.

AN10: As in AN1, but without stirring during the reaction (no magnetic bar used).

IS7: As in IS3, but now trioctylamine was used instead of oleylamine.

IS8: As in IS3, but now with only a "moderate" excess of oleylamine (12 equiv. to 1 equiv. Ni) and addition of ∼20 mL of anisole as a solvent.

AN11: As in AN7, but now the temperature is 215 °C for 1h.

AN12: As in AN11, but now 2 equiv. of HDA were also added to the 1 equiv. of Ni.

AN13: As in AN11, but $Ni(acac)_2$ replaced the Ni-acetate.

AN14: As in AN11, but Ni-acetate is replaced by Ni-stearate.

IS9: As in AN11, but Ni-acetate is replaced by $Ni(COD)_2$

AN15: As in AN12, but HDA is replaced by oleic acid.

AN16: As in AN11, but HDA is used as a solvent instead of oleylamine.

AN17: As in AN16, but Ni-acetate is replaced by $Ni(acac)_2$

AN18: As AN11, but 10 equiv. of trioctylphosphine oxide (TPPO) are added to the 1 equiv. of Ni.

AN19: As in AN12, but using hexadecane instead of OAm.

AN20: As in AN12, but HDA is replaced by 1-adamantanecarboxylic acid (ACA).

AN21: As in AN1, but 1 equiv. ACA is also added to the 2 equiv. of HDA.

IS10: $Ni(COD)_2$ decomposed in anisole, 3 bar H_2, 150 °C, 24h in the presence of ACA/HDA ligand mixture (1 equiv. Ni, 1 equiv. ACA, 2 equiv. HDA).

AN22: As in IS10, but $Ni(COD)_2$ was replaced by Ni-acetate.

AN23: As in AN22, but now $Ni(acac)_2$ was used as a precursor.

IS11: As AN19, but 1 equiv. ACA is also added to the 2 equiv. of HDA.

AN24: As in AN22, but with inversed ACA/HDA ratio (2/1).

AN25: As IS10, but with inversed ACA/HDA ratio (2/1).

AG1: As in AN25, but with the single use of ACA (no HDA used).

AN26: As in AN18, but TPPO is replaced by TOPO (trioctylphosphine oxide).

AN27: As in AN19, but the concentration of HDA is increased to 10 equiv.

AN28: As in AN8, but the octadecylamine was replaced by hexadecylamine.

AN29: As in AN18, but at 150 °C and for 48 h.

AN30: As in IS3, but TOPO was used as a solvent/surfactant instead of oleylamine.

■ ASSOCIATED CONTENT

Ⓢ Supporting Information

TEM and HRTEM images and XRD figure. This material is available free of charge via the Internet at http://pubs.acs.org.

■ AUTHOR INFORMATION

Corresponding Author

*E-mail:myrtil.kahn@lcc-toulouse.fr; pierre.fau@lcc-toulouse.fr.

Notes

The authors declare no competing financial interest

■ ACKNOWLEDGMENTS

The authors are grateful to the "Service Commun de Microscopie Electronique de L'Université Paul Sabatier" (TEMSCAN) for assistance in TEM/HRTEM/SEM. L. Vendier and A. Mari are acknowledged for XRD and SQuID measurements, respectively. This research was supported by the Centre National de la Recherche Scientifique, CNRS. This work was achieved in the frame of the French research program PREFACE (PRojet d'Etude Foudre sur Avion Composite plus Electrique). The authors thank the financing Ministries of Defense (DGA) and Industry (DGCIS) as well as the sponsors which are ASTECH, Hispano-Suiza; AESE, Safran Engineering Service; PEGASE, Eurocopter; and all partners involved in the project.

■ REFERENCES

(1) Lewis, L. N. Chemical catalysis by colloids and clusters. *Chem. Rev.* **1993**, *93*, 2693−2730.

(2) Somorjai, G. A. Modern Surface Science and Surface Technologies: An Introduction. *Chem. Rev.* **1996**, *96*, 1223−1236.

(3) *Handbook of Heterogeneous Catalysis* Ertl, G., Knozinger, H., Weitkamp, J., Eds.; Wiley-VCH: Weinheim, Germany, 2008.

(4) Taton, T. A.; Mirkin, C. A.; Letsinger, R. L. Scanometric DNA Array Detection with Nanoparticle Probes. *Science* **2000**, *289*, 1757−1760.

(5) Tkachenko, A. G.; Xie, H.; Coleman, D.; Glomm, W.; Ryan, J.; Anderson, M. F.; Franzen, S.; Feldheim, D. L. Multifunctional Gold Nanoparticle-Peptide Complexes for Nuclear Targeting. *J. Am. Chem. Soc.* **2003**, *125*, 4700−4701.

(6) Cheng, M. M. -C.; Cuda, G.; Bunimovich, Y. L.; Gaspari, M.; Heath, J. R.; Hill, H. D.; Mirkin, C. A.; Nijdam, A. J.; Terracciano, R.; Thundat, T.; Ferrari, M. Nanotechnologies for biomolecular detection and medical diagnostics. *Curr. Opin. Chem. Biol.* **2006**, *10*, 11−19.

(7) Wang, H.; Brandl, D. W.; Nordlander, P.; Halas, N. J. Plasmonic Nanostructures: Artificial Molecules. *Acc. Chem. Res.* **2007**, *40*, 53−62.

(8) Davey, N. M.; Seymour, R. J. The Platinum Metals in Electronics. *Platinum Metals Rev.* **1985**, *29*, 2−11.

(9) LaGrow, A. P.; Ingham, B.; Cheong, S.; Williams, G. V. M; Dotzler, C.; Toney, M. F.; Jefferson, D. A.; Corbos, E. C.; Bishop, P. T.; Cookson, J.; Tilley, R. D. Synthesis, Alignment, and Magnetic Properties of Monodisperse Nickel Nanocubes. *J. Am. Chem. Soc.* **2012**, *134*, 855−858.

(10) Mall, S.; Rodriguez, J.; Alexander, M. D. Electromagnetic Interference and electrical conductivity behavior of carbon/polycyanate composite with nickel nanostrands™ under fatigue. *Polym. Composite.* **2011**, *32*, 483−490.

(11) Chen, D. H.; Wu, S. H. Synthesis of Nickel Nanoparticles in Water-in-Oil Microemulsions. *Chem. Mater.* **2000**, *12*, 1354−1360.

(12) Krishnadas, K. R.; Sajanlal, P. R.; Pradeep, T. Pristine and Hybrid Nickel Nanowires: Template-, Magnetic Field-, and Surfactant-Free Wet Chemical Synthesis and Raman Studies. *J. Phys. Chem. C* **2011**, *115*, 4483−4490.

(13) Zhang, L. Y.; Wang, J.; Wei, L. M.; Liu, P.; Wei, H.; Zhang, Y. F. Synthesis of Ni nanowires via a hydrazine reduction route in aqueous ethanol solutions assisted by external magnetic fields. *Nano-Micro Lett.* **2009**, *1*, 49−52.

(14) Liu, Z.; Li, S.; Peng, S.; Hu, Z.; Qian, Y. Complex-Surfactant-Assisted Hydrothermal Route to Ferromagnetic Nickel Nanobelts. *Adv. Mater.* **2003**, *15*, 1946−1948.

(15) Zhou, W.; He, L.; Cheng, R.; Guo, L.; Chen, C.; Wang, J. Synthesis of Ni Nanochains with Various Sizes: The Magnetic and Catalytic Properties. *J. Phys. Chem. C* **2009**, *113*, 17355−17358.
(16) Libor, Z.; Zhang, Q. The synthesis of nickel nanoparticles with controlled morphology and SiO_2/Ni core-shell structures. *Mater. Chem. Phys.* **2009**, *114*, 902−907.
(17) Knez, M.; Bittner, A. M.; Boes, F.; Wege, C.; Jeske, H.; Maiss, E.; Kern, K. Biotemplate Synthesis of 3-nm Nickel and Cobalt Nanowires. *Nano Lett.* **2003**, *3*, 1079−1082.
(18) Kahn, M. L.; Glaria, A.; Pages, C.; Monge, M.; Saint-Macary, L.; Maisonnat, A.; Chaudret, B. Organometallic chemistry: an alternative approach towards metal oxide nanoparticles. *J. Mater. Chem.* **2009**, *19*, 4044−4060.
(19) Philippot, K.; Chaudret, B. *C. R. Chim.* **2003**, *6*, 1019−1034.
(20) Kahn, M. L.; Monge, M.; Collière, V.; Senocq, F.; Maisonnat, A.; Chaudret, B. Size- and Shape-Control of Crystalline Zinc Oxide Nanoparticles: A New Organometallic Synthetic Method. *Adv. Funct. Mater.* **2005**, *15*, 458−468.
(21) Dumestre, F.; Chaudret, B.; Amiens, C.; Respaud, M.; Fejes, P.; Renaud, P.; Zurcher, P. Unprecedented Crystalline Super-Lattices of Monodisperse Cobalt Nanorods. *Angew. Chem., Int. Ed.* **2003**, *42*, 5213−5216.
(22) Mourdikoudis, S.; Simeonidis, K.; Gloystein, K.; Angelakeris, M.; Dendrinou-Samara, C.; Tsiaoussis, I.; Kalogirou, O. Tailoring the morphology of Co_xPt_{1-x} magnetic nanostructures. *J. Magn. Magn. Mater.* **2009**, *321*, 3120−3125.
(23) Liakakos, N.; Cormary, B.; Li, X.; Lecante, P.; Respaud, M.; Maron, L.; Falqui, A.; Genovese, A.; Vendier, L.; Koinis, S.; Chaudret, B.; Soulantica, K. The Big Impact of a Small Detail: Cobalt Nanocrystal Polymorphism as a Result of Precursor Addition Rate during Stock Solution Preparation. *J. Am. Chem. Soc.* **2012**, *134*, 17922−17931.
(24) Carenco, S.; Boissière, C.; Nicole, L.; Sanchez, C.; Le Floch, P.; Mézailles, N. Controlled Design of Size-Tunable Monodisperse Nickel Nanoparticles. *Chem. Mater.* **2010**, *22*, 1340−1349.
(25) Shviro, M.; Zitoun, D. Nickel nanocrystals: fast synthesis of cubes, pyramids and tetrapods. *RSC Adv.* **2013**, *3*, 1380−1387.
(26) Cordente, N.; Amiens, C.; Chaudret, B.; Respaud, M.; Senocq, F.; Casanove, M.-J. Chemisorption on nickel nanoparticles of various shapes: Influence on magnetism. *J. Appl. Phys.* **2003**, *94*, 6358−6365.
(27) Cordente, N.; Respaud, M.; Senocq, F.; Casanove, M.-J.; Amiens, C.; Chaudret, B. Synthesis and Magnetic Properties of Nickel Nanorods. *Nano Lett.* **2011**, *1*, 565−568.
(28) Leng, Y.; Wang, Y.; Li, X.; Tiu, L.; Takahasshi, S. Controlled synthesis of triangular and hexagonal Ni nanosheets and their size-dependent properties. *Nanotechnology* **2006**, *17*, 4834−4839.
(29) Zhang, G.; Zhang, T.; Lu, X.; Wang, W.; Qu, J.; Li, X. Controlled Synthesis of 3D and 1D Nickel Nanostructures Using an External Magnetic Field Assisted Solution-Phase Approach. *J. Phys. Chem. C* **2007**, *111*, 12663−12668.
(30) Liu, Q.; Liu, H.; Han, M.; Zhu, J.; Liang, Y.; Xu, Z.; Song, Y. Nanometer-Sized Nickel Hollow Spheres. *Adv. Mater.* **2005**, *17*, 1995−1999.
(31) Bradley, J. S.; Tesche, B.; Busser, W.; Maase, M. Surface Spectroscopic Study of the Stabilization Mechanism for Shape-Selectively Synthesized Nanostructured Transition Metal Colloids. *J. Am. Chem. Soc.* **2000**, *122*, 4631−4636.
(32) Liu, D.; Ren, S.; Wu, H.; Zhang, Q.; Wen, L. Morphology control in synthesis of nickel nanoparticles in the presence of polyvinylpyrrolidone(PVPK30). *J. Mater. Sci.* **2008**, *43*, 1974−1978.
(33) Yang. L.; May, P. W.; Yin, L. In *Nanotechnology, Nanofabrication, Patterning and Self Assembly*; Dixon, C. J., Curtines, O. W., Eds.; Nova Science Publishers, Inc.: New York, 2010; pp 409−433, Chapter 12.
(34) Ramirez, E.; Eradès, L.; Philippot, K.; Lecante, P.; Chaudret, B. Shape Control of Platinum Nanoparticles. *Adv. Funct. Mater.* **2007**, *17*, 2219−2228.
(35) Singamaneni, S.; Bliznyuk, V. Fabrication of Ni nanoparticles and their size-selective self-assembly into chains under external magnetic field. *Appl. Phys. Lett.* **2005**, *87*, 162511(1)−162511(3).
(36) Martin, J. I.; Nogues, J.; Liu, K.; Vicent, J. L.; Schuller, I. K. Ordered magnetic nanostructures: fabrication and properties. *J. Magn. Magn. Mater.* **2003**, *256*, 449−501.
(37) Tzitzios, V.; Basina, G.; Gjoka, M.; Alexandrakis, V.; Georgakilas, V.; Niarchos, D.; Boukos, N.; Petridis, D. Chemical Synthesis and characterization of hcp Ni nanoparticles. *Nanotechnology* **2006**, *17*, 3750−3755.
(38) Donegan, K. P.; Godsell, J. F.; Otway, D. J.; Morris, M. A.; Roy, S.; Holmes, J. D. Size-tuneable synthesis of nickel nanoparticles. *J. Nanopart. Res.* **2012**, *14*, 670(1)−670(10).
(39) Ciuculescu, D.; Dumestre, F.; Comesana-Hermo, M.; Chaudret, B.; Spasova, M.; Farle, M.; Amiens, C. Single-Crystalline Co Nanowires: Synthesis, Thermal Stability, and Carbon Coating. *Chem. Mater.* **2009**, *21*, 3987−3995.
(40) Burton, W. K.; Cabrera, N.; Frank, F. C. The growth of crystals and the equilibrium structure of their surfaces. Royal Soc. London. *Philos. Trans.* **1951**, *A243*, 299−358.
(41) Dove, P. M.; Davis, K. J.; De Yoreo, J. J. In *Solid-Fluid Interfaces to Nanostructural Engineering*; Liu, X.Y., De Yoreo, J. J., Eds.; Kluewer/Plenum Academic Press: New York, 2004; Vol. *II*.
(42) Kashchiev, D. *Nucleation: Basic Theory with Applications*; Butterworths Heinemann: Oxford, 1999.
(43) Carbo-Argibay, E.; Rodriguez-Gonzalez, B.; Gomez-Grana, S.; Guerrero-Martinez, A.; Pastoriza-Santos, I.; Perez-Juste, J.; Liz-Marzan, L. M. The Crystalline Structure of Gold Nanorods Revisited: Evidence for Higher-Index Later Facets. *Angew. Chem., Int. Ed.* **2010**, *49*, 9397−9400.
(44) Huo, Z.; Tsung, C.-k.; Huang, W.; Zhang, X.; Yang, P. Sub-Two Nanometer Single Crystal Au Nanowires. *Nano Lett.* **2008**, *8*, 2041−2044.
(45) You, Y.; Kondoh, H.; Che, R.; Takeguchi, M.; Ohta, T. Ferromagnetic FePt Nanowires: Solvothermal Reduction Synthesis and Characterization. *Small* **2006**, *2*, 235−238.
(46) Zhang, Z.; Blom, D. A.; Gai, Z.; Thompson, J. R.; Shen, J.; Dai, S. High-Yield Solvothermal Formation of Magnetic CoPt Alloy Nanowires. *J. Am. Chem. Soc.* **2003**, *125*, 7528−7529.
(47) Chang, Y.; Lye, M. L.; Zeng, H. C. Large-Scale Synthesis of High-Quality Ultralong Copper Nanowires. *Langmuir* **2005**, *21*, 3746−3748.
(48) Axet, M. R.; Philippot, K.; Chaudret, B.; Cabie, M.; Giorgio, S.; Henry, C. R. TEM and HRTEM Evidence for the Role of Ligands in the Formation of Shape-Controlled Platinum Nanoparticles. *Small* **2011**, *7*, 235−241.
(49) The decomposition of $Ni(COD)_2$ corresponds to the hydrogenation of the cyclooctadiene that releases the Ni(0) atoms while the reduction of Ni(II) complexes will certainly involve several steps as recently reported for the $Ni(acac)_2$ reduction by amines. See for example: Carenco, S.; Labouille, S.; Bouchonnet, S.; Boissiere, C.; Le Goff, X. F.; Sanchez, C.; Mezailles, N. Revisiting the Molecular Roots of a Ubiquitously Successful Synthesis: Nickel(0) Nanoparticles by Reduction of $[Ni(acetylacetonate)_2]$. *Chem.—Eur. J.* **2012**, *18*, 14165−14173.
(50) Park, K. H.; Jang, K.; Kim, H. J.; Son, S. U. Near-Monodisperse Tetrahedral Rhodium Nanoparticles on Charcoal: The Shape Dependent Catalytic Hydrogenation of Arenes. *Angew. Chem., Int. Ed.* **2007**, *46*, 1152−1155.
(51) Zhang, H.-T.; Ding, J.; Chow, G.-M. Morphological Control of Synthesis and Anomalous Magnetic Properties of 3-D Branched Pt Nanoparticles. *Langmuir* **2008**, *24*, 375−378.
(52) Kotoulas, A.; Gjoka, M.; Simeonidis, K.; Tsiaoussis, I.; Angelakeris, M.; Kalogirou, O.; Dendrinou-Samara, C. The role of synthetic parameters in the magnetic behavior of relative large hcp Ni nanoparticles. *J. Nanopart. Res.* **2011**, *13*, 1897−1908.
(53) Chen, Y.; Peng, D.-L.; Lin, D.; Luo, X. Preparation and magnetic properties of nickel nanoparticles via the thermal decomposition of nickel organometallic precursor in alkylamines. *Nanotechnology* **2007**, *18*, 505703(1)−505703(6).
(54) Typically temperatures over 215 °C are sufficient for the complete and fast decomposition of most nickel precursors with our

reaction conditions; 150 °C are also enough providing that we use dihydrogen for a long reaction time. Upon the end of the reaction, the supernatant is normally transparent, and the black product is collected on the stirring magnet.

(55) Yong, K.-T.; Sahoo, Y.; Swihart, M. T.; Prasad, P. N. Shape Control of CdS Nanocrystals in One-Pot Synthesis. *J Phys. Chem. C* **2007**, *111*, 2447−2458.

(56) LaGrow, A. P.; Cheong, S.; Watt, J.; Ingham, B.; Toney, M. F.; Jefferson, D. A.; Tilley, R. D. Can Polymorphism be Used to form Branched Metal Nanostructures? *Adv. Mater.* **2013**, *25*, 1552−1556.

(57) Zhang, L.; Dou, Y.-H.; Gu, H.-C. Sterically induced shape control of magnetite nanoparticles. *J. Cryst. Growth* **2006**, *296*, 221−226.

(58) Shevchenko, E. V.; Talapin, D. V.; Rogach, A. L.; Kornowski, A.; Haase, M.; Weller, H. Colloidal Synthesis and Self-Assembly of $CoPt_3$ Nanocrystals. *J. Am. Chem. Soc.* **2002**, *124*, 11480−11485.

(59) Shen, S.; Zhuang, J.; Xu, X.; Nisar, A.; Hu, S.; Wang, X. Size Effects in the Oriented-Attachment Growth Process: The Case of Cu nanoseeds. *Inorg. Chem.* **2009**, *48*, 5117−5128.